

# Optical measurement of material abundances in mixtures incorporating preprocessing to mitigate spectral variability

Wolfgang Krippner, Sebastian Bauer and Fernando Puente León

Institute of Industrial Information Technology (IIIT),  
Karlsruhe Institute of Technology (KIT),  
Hertzstr. 16, 76187 Karlsruhe, Germany

**Abstract** A new optical approach for determining the abundances of substances in mixtures is presented. By using specifically designed spectral filters, it is sufficient to acquire monochrome images whose intensity quantitatively depicts the abundance of the respective material.

**Keywords:** Hyperspectral image, optical computing, optical measurement, spectral filtering.

## 1 Introduction

Hyperspectral images allow for the extraction of rich information about the considered scene. The downside of hyperspectral imaging, however, is the high cost for acquisition devices and the subsequent elaborate image processing hardware and software. In this paper, we investigate an alternative approach to spectral unmixing based on recorded images. Spectral unmixing denotes the process of extracting the material abundances in mixtures. Bypassing the need for acquisition, processing and information extraction, we use programmable spectral filters that allow for the acquisition of a single intensity image. When the spectral filter is chosen adequately, this image encodes the spatial abundance of the considered target spectrum. We present filter design methods that take the spectral variability of the target spectra into account.

## 2 Spectral filter design methods

The optical measurement of material abundances in mixtures uses specifically designed spectral filters. Their calculation is described in this section. Their implementation will be discussed in Section 4. Each of the following methods for the analytical design of spectral filters is based on the linear mixing model (LMM)

$$\mathbf{y}_{ij} = \sum_{k=1}^p a_{ijk} \mathbf{m}_k + \varepsilon_{ij} = \hat{\mathbf{y}}_{ij} + \varepsilon_{ij}, \quad (9.1)$$

where  $\mathbf{y}_{ij}$  denotes the spectrum at pixel  $i, j$  of the hyperspectral image  $\mathbf{Y} \in \mathbb{R}^{n_x \times n_y \times \Lambda}$  and  $\mathbf{Y} \geq \mathbf{0}$ , measured at  $\Lambda$  wavelengths. The spectra of the  $p$  pure materials assumed to be present in the observed scene are described by  $\mathbf{m}_k$ , whereas the  $a_{ijk}$  denote the corresponding abundances. To account for a physically meaningful representation, the abundances are commonly restricted by the constraints  $\sum_{k=1}^p a_{ijk} = 1$  and  $a_{ijk} \geq 0 \forall i, j, k$ . Both measurement noise and deviations from solely linear mixing are taken into account by  $\varepsilon_{ij}$ .

The following methods for the design of spectral filters assume that the  $\mathbf{m}_k$  are known, whereas  $\mathbf{Y}$  is not recorded and, consequently, not available for any subsequent derivations. Particularly, for each material  $k$ , a collection of  $n$  spectra  $\mathbf{m}_{kl}$  ( $l = 1, \dots, n$ ) exists in addition to the corresponding mean spectrum  $\mathbf{m}_k^*$ . The differences between the  $\mathbf{m}_{kl}$  within the collection are mainly the result of chemical, microscopic and macroscale geometric effects. The so-called endmember variability [1] denotes this variability of pixel spectra of the same pure material and will be considered by an instability index [2, 3], which is used as a preprocessing step for the endmember collections in some of the next derivations of the spectral filters.

Following the LMM (9.1), the mathematical derivation of material abundances results in

$$a_{ijk} = \mathbf{f}_k^T \mathbf{y}_{ij} = \sum_{k=1}^p a_{ijk} \mathbf{f}_k^T \mathbf{m}_k, \quad (9.2)$$

where  $\mathbf{f}_k$  denotes the spectral filter used to obtain the abundances of the pure material  $k$  assuming  $\varepsilon_{ij} = 0$ . The determination of the abundances in (9.2) will be performed optically. It should be noted that

(9.2) obviously stipulates both  $\mathbf{f}_k^T \mathbf{m}_k = 1$  and  $\mathbf{f}_k^T \mathbf{m}_j = 0$  for  $k \neq j$  and  $j = 1, 2, \dots, p$ . However, not only  $\varepsilon_{ij} \neq 0$ , but also the endmember variability substantially hamper that these conditions be exactly fulfilled.

As a general method for deriving  $\mathbf{f}_k$ , we consider the least-squares estimator. Using (9.1) and performing some further calculations, omitted for the sake of space, leads to

$$\mathbf{a}_{ij} = \begin{bmatrix} a_{ij1} \\ \vdots \\ a_{ijp} \end{bmatrix} = \begin{bmatrix} \mathbf{f}_1^T \\ \vdots \\ \mathbf{f}_p^T \end{bmatrix} \mathbf{y}_{ij} = (\mathbf{M}^T \mathbf{M})^{-1} \mathbf{M}^T \mathbf{y}_{ij}, \quad (9.3)$$

where  $\mathbf{M} = [\mathbf{m}_1, \dots, \mathbf{m}_p]$  holds and  $(\mathbf{M}^T \mathbf{M})^{-1} \mathbf{M}^T$  is called the *Moore–Penrose pseudoinverse* of  $\mathbf{M}$ .

The design of spectral filters according to (9.3), where  $\mathbf{M}$  is replaced by  $\mathbf{M}^* = [\mathbf{m}_1^*, \dots, \mathbf{m}_p^*]$ , describes the first method considered for the optical determination of material abundances. The spectral filters derived by this method are denoted as *pseudoinverse spectral filters*  $\mathbf{f}_k^{\text{PS}}$ . In contrast, the following methods first apply the spectral manipulation  $\mathbf{C} \mathbf{y}_{ij} = \mathbf{C} \mathbf{M} \mathbf{a}_{ij}$ , where  $\mathbf{C} \in \mathbb{R}^{\Lambda \times \Lambda}$  denotes a non-orthogonal matrix. Then, the spectral filters are derived by

$$\tilde{\mathbf{a}}_{ij} = \begin{bmatrix} \tilde{a}_{ij1} \\ \vdots \\ \tilde{a}_{ijp} \end{bmatrix} = \begin{bmatrix} \tilde{\mathbf{f}}_1^T \\ \vdots \\ \tilde{\mathbf{f}}_p^T \end{bmatrix} \mathbf{y}_{ij} = ((\mathbf{C} \mathbf{M})^T \mathbf{C} \mathbf{M})^{-1} (\mathbf{C} \mathbf{M})^T \mathbf{C} \mathbf{y}_{ij} \quad (9.4)$$

denoting a similar approach as (9.3).

Searching for a meaningfully defined  $\mathbf{C}$ , [3] proposes to account for the shape of  $\mathbf{m}_k$  in order to improve the estimates of the material abundances. Spectral differences  $\Delta m_{ki} = m_{ki+1} - m_{ki}$  ( $i = 1, \dots, \Lambda - 1$ ) leading to spectra  $\Delta \mathbf{m}_k$  are calculated therefor. This can be performed by a suitably chosen  $\mathbf{C}$ . Applying the differences on material spectra tends to significantly increase the endmember variability. To mitigate this drawback, we smooth each spectrum beforehand by applying the discrete cosine transform [4] first and then removing coefficients representing high frequencies. Note that the discrete cosine transform is a linear transformation and, consequently, can be integrated into an

appropriate  $\mathbf{C}$ . The spectral filters, named *differential filters*  $\Delta\tilde{\mathbf{f}}_k$  in the following, finally result by using  $\mathbf{C} = \mathbf{C}_{\text{diff}}\mathbf{C}_{\text{dct}}^T\mathbf{C}_{\text{sm}}\mathbf{C}_{\text{dct}}$ , where  $\mathbf{C}_{\text{dct}} \in \mathbb{R}^{\Lambda \times \Lambda}$  denotes the discrete cosine transform matrix.  $\mathbf{C}_{\text{sm}} \in \mathbb{R}^{\Lambda \times \Lambda}$  denotes the identity matrix, where  $c_{\text{sm},mn} = 0$  for  $n = m, \dots, \Lambda$  for the  $m$  highest frequencies that belong to sharp edges of  $\mathbf{m}_k$  and therefore should be suppressed. The matrix  $\mathbf{C}_{\text{diff}} \in \mathbb{R}^{\Lambda \times \Lambda}$  is used to derive  $\Delta\mathbf{m}_k$ , where  $\Delta\mathbf{m}_k^*$  denotes the differences of the mean spectra that are considered for  $\Delta\tilde{\mathbf{f}}_k$ .  $\mathbf{C}_{\text{diff}}$  consists of ones on the main diagonal and  $-1$  on the first diagonal above the main diagonal.

The next methods for the derivation of the spectral filters extend  $\mathbf{f}_k^{\text{PS}}$  and  $\Delta\tilde{\mathbf{f}}_k$  to incorporate the endmember variability contained within the collections of the pure materials. In detail, the endmember variability is valued by the instability index, abbreviated with ISI, and defined as

$$\text{ISI}_\lambda = \frac{\Delta_{\text{within } \lambda}}{\Delta_{\text{between } \lambda}} = \frac{P}{P-1} \sum_{k=1}^{P-1} \sum_{r=k+1}^P \frac{1.96 (\sigma_{k\lambda} - \sigma_{r\lambda})}{|R_{\text{mean},k\lambda} - R_{\text{mean},r\lambda}|} \quad (9.5)$$

for each wavelength  $\lambda = 1, \dots, \Lambda$ . In this equation,  $R_{\text{mean},k\lambda}$  denotes the mean reflectance value of class  $k$  at wavelength  $\lambda$  and  $\sigma_{k\lambda}$  the standard deviation of class  $k$  at the same wavelength.

The variability at wavelength  $\lambda$  within each collection of spectra referring to a certain material class is taken into account by  $\Delta_{\text{within } \lambda}$ , whereby the sum of the one-sided 95 % confidence interval is used under the assumption that each collection contains normally distributed spectra. Conversely,  $\Delta_{\text{between } \lambda}$  accounts for the distances between the mean spectra of the pure materials  $k$  and  $r$  at wavelength  $\lambda$ , i.e.,  $m_{k\lambda}^*$  and  $m_{r\lambda}^*$ . Using (9.5) allows to assess the endmember variability at each wavelength. A large value of  $\text{ISI}_\lambda$  indicates a greater value of  $\Delta_{\text{within } \lambda}$  than the value of  $\Delta_{\text{between } \lambda}$ . Wavelength  $\lambda$  should consequently be discarded for the design of the spectral filters.

To incorporate the ISI index into the filter design (9.4), we propose two different versions of the transformation matrix  $\mathbf{C}$ . The first one uses (9.5) for defining additional weightings for each wavelength by

$$\mathbf{C}_{\text{ISI}} = \begin{bmatrix} \text{ISI}_1^{-1} & 0 & \dots & 0 \\ 0 & \text{ISI}_2^{-1} & 0 & \dots & 0 \\ \vdots & \ddots & \ddots & \ddots & \vdots \\ 0 & \dots & 0 & \text{ISI}_\Lambda^{-1} \end{bmatrix} \in \mathbb{R}^{\Lambda \times \Lambda}, \quad (9.6)$$

whereas the second one not only considers these weightings, but also completely removes wavelengths corresponding to high values of (9.5) by using  $\mathbf{C}_{\text{ISI,Thresh}} = \mathbf{C}_{\text{Thresh}} \mathbf{C}_{\text{ISI}}$ . Here,  $\mathbf{C}_{\text{Thresh}} \in \mathbb{R}^{\Lambda \times \Lambda}$  denotes a unit matrix with  $c_{\text{Thresh},ii} = 0$  if  $\text{ISI}_\lambda > \tau$  holds. For the threshold  $\tau$  we consider a multiple of the mean of the ISI,  $\tau = c \mu_{\text{ISI}}$  and  $c > 0$ .

Combining  $\mathbf{C}_{\text{ISI}}$  and  $\mathbf{C}_{\text{ISI,Thresh}}$  with  $\mathbf{f}_k$  and  $\Delta \mathbf{f}_k^{\text{PS}}$  is achieved by setting  $\mathbf{C} = \mathbf{C}_{\text{ISI}}$ ,  $\mathbf{C} = \mathbf{C}_{\text{ISI,Thresh}}$  and  $\mathbf{C} = \mathbf{C}_{\text{ISI}} \mathbf{C}_{\text{diff}} \mathbf{C}_{\text{dct}}^T \mathbf{C}_{\text{sm}} \mathbf{C}_{\text{dct}}$ ,  $\mathbf{C} = \mathbf{C}_{\text{ISI,Thresh}} \mathbf{C}_{\text{diff}} \mathbf{C}_{\text{dct}}^T \mathbf{C}_{\text{sm}} \mathbf{C}_{\text{dct}}$ , respectively, and yields the spectral filters denoted by  $\tilde{\mathbf{f}}_k^{\text{PS,ISI}}$ ,  $\tilde{\mathbf{f}}_k^{\text{ISI,Th}}$ ,  $\Delta \tilde{\mathbf{f}}_k^{\text{ISI}}$  and  $\Delta \tilde{\mathbf{f}}_k^{\text{ISI,Th}}$ .

In total, 6 types of spectral filters have been presented. The following section shows our approach for their optical implementation, whereas in Section 4, each of them is applied experimentally to evaluate its performance in estimating material abundances.

### 3 Optical implementation of spectral filters

In order to realize the spectral filters derived in the previous section, we customize the measuring system which is normally used to record common hyperspectral images. The following measuring approach results in an innovative procedure for deriving material abundances in mixtures.

Hyperspectral images are obtained by first discretizing the considered wavelength range into a finite number of wavelength channels. The scalar images, which finally form a hyperspectral image by arranging them to a stack, are then measured with a constant exposure time in each wavelength channel. Thus, each wavelength is weighted equally. Conversely, to optically realize the designed spectral filters, we adjust the exposure time of each wavelength channel with respect to the spectral filter coefficients. Large values in the magnitudes of the coefficients result in higher exposure times and vice versa. Eventually, the grayscale intensity images only have to be summed up in order to obtain spatial estimates for the material abundances. Note that keeping the camera shutter open during the complete measuring time even supersedes the need for recording numerous grayscale images and summing them up, and directly yields the intensity image showing the material abundances. Because of hardware restrictions,

this advanced exposure technique has not been investigated experimentally yet, though.

Since negative values of spectral filter coefficients may occur, whereas physically meaningful exposure times are restricted to positive values, the spectral filters have to be split into a positive and a negative part,  $\mathbf{f}_k = \mathbf{f}_k^+ + \mathbf{f}_k^-$ , where  $f_{k\lambda}^+ \geq 0$  and  $f_{k\lambda}^- < 0$  hold for  $\lambda = 1, 2, \dots, \Lambda$ . Hence, instead of  $\mathbf{f}_k$ , two grayscale images are recorded that represent the optical realization of  $\mathbf{f}_k^+$  and  $\mathbf{f}_k^-$ . As mandatory postprocessing step, they have to be subtracted.

## 4 Experimental evaluation

For the evaluation of the optical determination of material abundances in mixtures we used an experimental setup consisting of a 300 W Xenon lamp as the light source, an EMCCD camera (Andor iXon<sub>3</sub>897) and a spectral filter, namely an acousto-optical tunable filter (AOTF, Gooch&Housego HSi-300), which allows to tune the mean wavelength and bandwidth of each wavelength channel. The following evaluations consider the wavelength range between 450 and 810 nm, in which the sampling is accomplished in steps of 4 nm resulting in 91 wavelength channels.

As samples we examine mixtures of color powders and mixtures created by a laser printer with reference to an artificially derived image. The additional investigation of the second mixture scheme results from former examinations, which exhibit significant violations of the LMM by mixtures of color powders. In contrast, the printed mixtures approximate the LMM sufficiently well due to the fact that they were designed aiming for meeting assumptions belonging to the LMM, such as that spectral mixing occurs only on the macroscopic scale [5]. The determination of the material abundances with the printed mixtures remains challenging because the number of raw materials is increased by a fifth color.

Since in each mixture regions including a single material are present, spectra of the corresponding pixels are used to build the collections of spectra of pure materials. The mean spectra and variances are shown in Figures 9.1 and 9.2. Note that the spectrum of color 5 exhibits a remarkable similarity to the spectrum of color 2, whereas the pure spec-

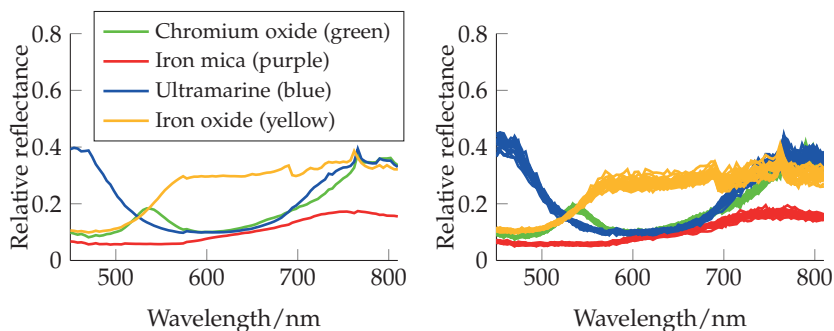


**Figure 9.1:** Powder mixtures: mean spectra (left), 20 pixel samples of pure spectra as an excerpt of the used collections (right).

tra within the mixture of the color powders are visually more distinguishable. The variances demonstrate notable endmember variability throughout the considered wavelength range. Using the information about ultramarine, Figure 9.3 illustrates the normalized (i.e., the maximum value is normalized to 1) spectral filters following from Section 2. Though the spectral filters aim for estimating the abundances of the same material, their shapes vary substantially.

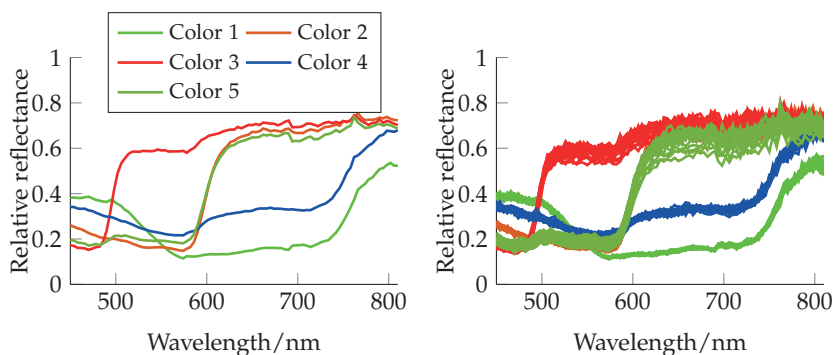
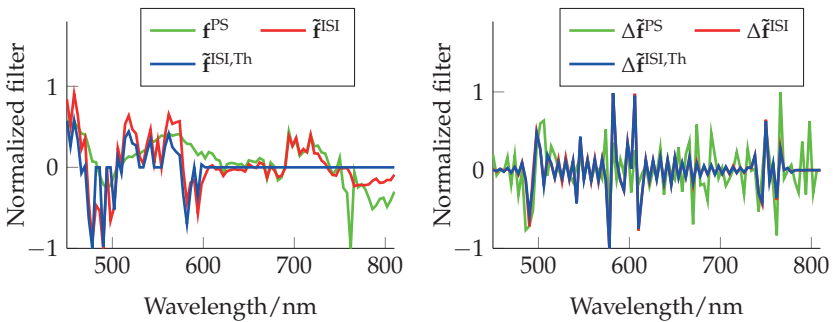


**Figure 9.2:** Printed mixtures: mean spectra (left), 20 pixel samples of pure spectra as an excerpt of the used collections (right).

The assessment of the spectral filters' performance in accurately estimating material abundances is conducted using the root mean square error  $e_\theta = \frac{1}{n_x n_y} \sqrt{\sum_{i=1}^{n_x} \sum_{j=1}^{n_y} \theta_{ij}^2}$  where  $\theta_{ij}$  denotes the angle between the estimated abundances  $\hat{\mathbf{a}}_{ij}$  and the true abundances  $\mathbf{a}_{ij}$  (ground truth) at pixel  $i, j$ , calculated by  $\theta_{ij} = \hat{\mathbf{a}}_{ij}^T \mathbf{a}_{ij} / \|\hat{\mathbf{a}}_{ij}\| \|\mathbf{a}_{ij}\|$ . The root mean square error is invariant to the normalization of  $\hat{\mathbf{a}}_{ij}$  [6] and therefore provides qualitative results. It will be used to evaluate both the optically determined abundances and the abundances derived by mathematically applying the spectral filters on recorded full hyperspectral images of the mixtures.

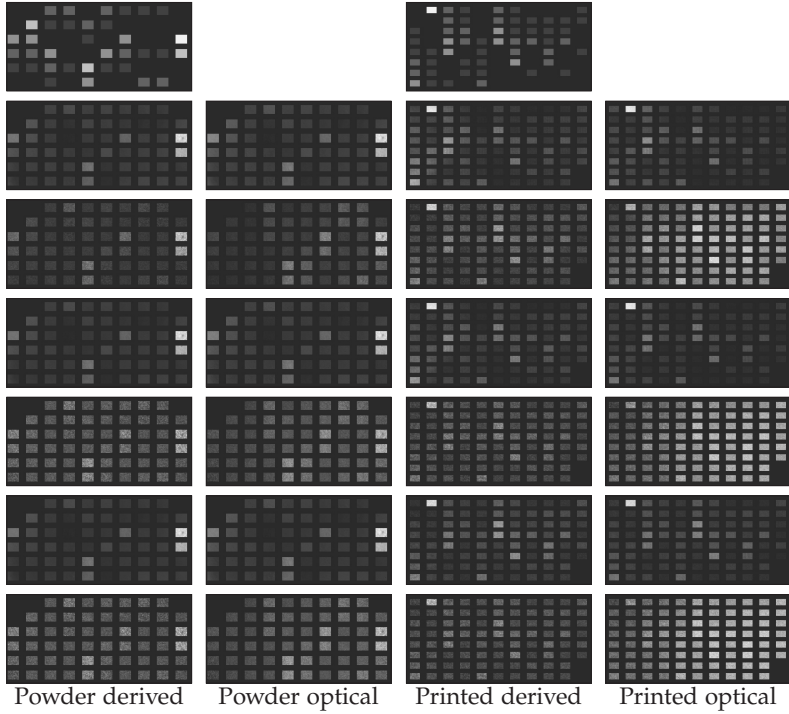
Tables 9.1 and 9.2 show the results of  $e_\theta$  for both mixing schemes. In addition, the intensity images following from the use of the spectral filters for ultramarine and color 3, as illustrative examples, are presented in Figure 9.4. The evaluation exhibits slight differences of  $e_\theta$  with respect to the application of different spectral filters for the determination of material abundances.

Figure 9.4 allows the implication that the optical use of spectral filters based on shapes of the pure spectra leads to the largest deviations comparing with the derived results. Probably, the differences depend on the shape of the spectral filters. As a consequence, efforts for more detailed investigations focusing on the capability of the optical implementation of different types of shapes of spectral filters including comparisons with derived results, should be taken in future work.



**Figure 9.3:** Ultramarine: spectral filters using the original spectra (left) and their differences (right).





**Figure 9.4:** The two left columns show the ultramarine abundances, while the two right columns show the abundances of color 3. Top row: ground truth, second row: pure pseudoinverse ( $\mathbf{f}_k^{\text{PS}}$ ), third row: differences ( $\Delta \tilde{\mathbf{f}}_k$ ), fourth row: ISI index ( $\tilde{\mathbf{f}}_k^{\text{PS,ISI}}$ ), fifth row: ISI index with differences  $\Delta \tilde{\mathbf{f}}_k^{\text{ISI}}$ , sixth row: ISI index with threshold ( $\tilde{\mathbf{f}}_k^{\text{ISI,Th}}$ ), last row: ISI index with threshold and differences ( $\Delta \tilde{\mathbf{f}}_k^{\text{ISI,Th}}$ ).

## 5 Summary

The use of spectral filters for directly acquiring abundances in mixtures using grayscale images has been shown both theoretically and experimentally. Various filter design methods demonstrating some of the possibilities for incorporating additional information have been de-

**Table 9.1:** Powder mixtures: root mean square error.

	$\mathbf{f}^{\text{PS}}$	$\Delta\tilde{\mathbf{f}}$	$\tilde{\mathbf{f}}^{\text{ISI}}$	$\Delta\tilde{\mathbf{f}}^{\text{ISI}}$	$\tilde{\mathbf{f}}^{\text{ISI,Th}}$	$\Delta\tilde{\mathbf{f}}^{\text{ISI,Th}}$
$e_\theta$ optical	0.0001	0.0020	0.0001	0.0023	0.0001	0.0023
$e_\theta$ derived	0.0011	0.0010	0.0011	0.0013	0.0011	0.0013

**Table 9.2:** Printed mixtures: root mean square error.

	$\mathbf{f}^{\text{PS}}$	$\Delta\tilde{\mathbf{f}}$	$\tilde{\mathbf{f}}^{\text{ISI}}$	$\Delta\tilde{\mathbf{f}}^{\text{ISI}}$	$\tilde{\mathbf{f}}^{\text{ISI,Th}}$	$\Delta\tilde{\mathbf{f}}^{\text{ISI,Th}}$
$e_\theta$ optical	0.0017	0.0013	0.0016	0.0015	0.0012	0.0015
$e_\theta$ derived	0.0013	0.0010	0.0011	0.0013	0.0001	0.0013

scribed, e.g., the ISI index has been used that evaluates endmember variability. Although the results point into the right direction, filter design improvements have to be achieved in future. One possibility would be to include the conditions that the abundances of each pixel should be nonnegative and sum to one.

## References

1. B. Somers, G. P. Asner, L. Tits, and P. Coppin, "Endmember variability in spectral mixture analysis: A review," *Remote Sensing of Environment*, vol. 115, no. 7, pp. 1603–1616, April 2011.
2. B. Somers, M. Zortea, A. Plaza, and G. P. Asner, "Automated extraction of image-based endmember bundles for improved spectral unmixing," *IEEE Journal of Selected Topics in Applied Earth Observations and Remote Sensing*, vol. 5, no. 2, pp. 396–408, April 2012.
3. B. Somers, S. Delalieux, W. W. Verstraeten, J. A. N. van Aardt, G. L. Albrigo, and P. Coppin, "An automated waveband selection technique for optimized hyperspectral mixture analysis," *International Journal of Remote Sensing*, vol. 31, no. 20, pp. 5549–5568, October 2010.
4. N. Ahmed, T. Natarajan, and K. R. Rao, "Discrete cosine transform," *IEEE Transactions on Computers*, vol. C-23, no. 1, pp. 90–93, Jan 1974.
5. N. Keshava and J. F. Mustard, "Spectral unmixing," *IEEE Signal Processing Magazine*, vol. 19, no. 1, pp. 44–57, Jan 2002.
6. J. M. P. Nascimento and J. M. B. Dias, "Vertex component analysis: a fast algorithm to unmix hyperspectral data," *IEEE Transactions on Geoscience and Remote Sensing*, vol. 43, no. 4, pp. 898–910, April 2005.